J. Fluid Mech. (2012), *vol.* 709, *pp.* 396–407.
doi:10.1017/jfm.2012.341

Transition to turbulence at the bottom of a solitary wave

Paolo Blondeaux†, Jan Pralits and Giovanna Vittori

Department of Civil, Environmental and Architectural Engineering, Genoa University, via Montallegro 1, 16145 Genova, Italy

(Received 29 November 2011; revised 18 April 2012; accepted 2 July 2012; first published online 24 August 2012)

A linear stability analysis of the laminar flow in the boundary layer at the bottom of a solitary wave is made to determine the conditions leading to transition and the appearance of turbulence. The Reynolds number of the phenomenon is assumed to be large and a 'momentary' criterion of instability is used. The results show that the laminar regime becomes unstable during the decelerating phase, when the height of the solitary wave exceeds a threshold value which depends on the ratio between the boundary layer thickness and the local water depth. A comparison of the theoretical results with the experimental measurements of Sumer *et al.* (*J. Fluid Mech.*, vol. 646, 2010, pp. 207–231) supports the analysis.

Key words: boundary layer stability, coastal engineering, solitary waves

1. Introduction

To quantify sediment transport under sea waves, it is necessary to have a detailed knowledge of the boundary layer generated close to the bottom by wave propagation (Blondeaux & Vittori 1999). Hence, the appearance of turbulence and the turbulence structure in wave boundary layers have been extensively studied both using direct numerical simulations of continuity and Navier–Stokes equations (Verzicco & Vittori 1996; Vittori & Verzicco 1998) and by means of the Reynolds-averaged approach and turbulence models (e.g. Blondeaux 1987; Fredsoe & Deigaard 1992 and references therein). Indeed, coherent vortex structures and turbulent eddies play a crucial role in the pick-up of sediments and in their transport (Costamagna, Vittori & Blondeaux 2003; Vittori 2003; Mazzuoli, Vittori & Blondeaux 2011). However, most of these studies are restricted to linear waves and the results cannot be applied to the nearshore region where the water depth is much smaller than the length of the waves and wave asymmetry is significant. Recently, a few theoretical and experimental investigations have been carried out of the boundary layer generated by cnoidal waves and solitary waves (e.g. Tanaka, Sumer & Lodahl 1998; Sumer *et al.* 2010). In fact, as sea waves move from deep water to the shallow water region, the cnoidal wave and solitary wave theories are more appropriate to describe wave dynamics. Liu & Orfilia (2004) introduced the Boussinesq approximation and derived depth-integrated continuity and momentum equations for transient long waves. The resulting equations are differential–integral equations, in terms of the depth-averaged horizontal velocity and the free surface displacement, in which viscous effects are taken into account

† Email address for correspondence: blx@dicat.unige.it

by convolution integrals. Liu, Park & Cowen (2007), using the solution of Liu & Orfilia (2004), examined the boundary layer under a solitary wave and found that the velocity inside the bottom boundary layer reverses its direction during the decelerating phase, even though the free stream velocity always points in the direction of wave propagation. Consequently, the bed shear stress as well as the sediment transport rate change sign during the decelerating phase. However, the analysis considers the laminar flow regime. The velocity field in the turbulent boundary layer under a solitary wave was obtained by Vittori & Blondeaux (2008, 2011) by means of direct numerical simulations. A local model was developed which assumes that turbulence structure within the boundary layer is not affected by the slow spatial variations of the external flow. The obtained results show that, for small wave heights, the flow regime is laminar. Turbulence appears when the wave height becomes larger than a critical value which depends on the ratio between the boundary layer thickness and the water depth. Close to the critical conditions, turbulence is generated only during the decelerating phase or, conversely, turbulence is present only behind the wave crest. Only far from the critical conditions is turbulence generated also during the accelerating phase (Blondeaux & Vittori 2012). As already pointed out, even though the horizontal velocity component far from the bed always points in the direction of wave propagation, both the fluid velocity near the bottom and the bed shear stress reverse their direction when the irrotational velocity decelerates. The strength and length of time of flow reversal turn out to be affected by the appearance of turbulence. The numerical findings have been confirmed by the recent laboratory measurements of Sumer *et al.* (2010). The experimental results show that three flow regimes take place in the boundary layer generated by a solitary wave, depending on the value of the Reynolds number Re defined by Sumer *et al.* (2010) as $Re = 4H^{3/2}/(\sqrt{3}\delta^2)$, where H is the ratio between the wave height and the water depth h^* and δ is the ratio between the boundary layer thickness and h^*. For Reynolds numbers smaller than 2×10^5, the measured values of the velocity and the bed shear stress do not show any significant deviation from the laminar solution of Liu *et al.* (2007). As the value of Re is increased, in the range $(2 \times 10^5, 5 \times 10^5)$ and during the decelerating phase, the bed shear stress shows a sudden decrease followed by a strong increase. These oscillations are related to the appearance of quasi-two-dimensional vortex tubes clearly shown by the movies which are available at http://dx.doi.org/10.1017/S0022112009992837, in the supplementary material of the paper by Sumer *et al.* (2010). An increase of the Reynolds number above 5×10^5 leads to the appearance of multiple irregular spikes in the measured values of the bed shear stress, which are produced by the appearance of turbulent spots, moving areas of irregular turbulent eddies. As pointed out by Sumer *et al.* (2010), so far no study is available that investigate (from the point of view of hydrodynamic stability theory) the stability of the laminar regime in the boundary layer under a solitary wave. In the present work, we study the stability of the laminar boundary layer generated by the propagation of a solitary wave using a 'momentary' criterion for instability of the kind introduced by Shen (1961) and applied by Blondeaux & Seminara (1979) to investigate the stability of the Stokes boundary layer. We assume that transition takes place for large values of the Reynolds number such that it is reasonable to consider the time development of perturbations of the basic laminar flow, assuming that their growth takes place on a time scale much faster than the time scale of the basic flow. Moreover, a normal mode decomposition is applied and the investigation is carried out for the generic Fourier component. Finally, because Conrad & Criminale (1965) showed that two-dimensional perturbations are more unstable than three-dimensional perturbations even in unsteady

flows, the analysis considers only the former. Needless to say that the analysis can explain the appearance of the vortex tubes observed by Sumer *et al.* (2010) and predict their main characteristics (e.g. spacing), but it is unable to provide any information on the turbulent spots which are irregular three-dimensional vortex structures that can be investigated only by means of a fully nonlinear analysis.

The procedure used in the rest of the paper is as follows. In the next section we formulate the hydrodynamic problem and we describe the basic flow, i.e. the solution describing the velocity field induced by the propagation of a solitary wave. The solution is given both in the region where the fluid behaves like an inviscid fluid and close to the bottom where a viscous boundary layer develops. In § 3, we describe the linear stability analysis of the basic flow in the bottom boundary layer. The results are described in § 4 where a qualitative and quantitative comparison of the theoretical predictions with the laboratory measurements of Sumer *et al.* (2010) is also made. The conclusions are drawn in § 5.

2. Formulation of the problem and basic flow

A long two-dimensional solitary wave of height H^* propagates on a constant water depth h^* along the X_1^*-direction (a star denotes a dimensional quantity), the Cartesian coordinate system (X_1^*, X_2^*, X_3^*), having the (X_1^*, X_3^*)-plane coincident with the bottom and the X_2^*-axis pointing in the upward direction, is introduced. Assuming large values of the Reynolds number of the phenomenon, the flow field can be split into three regions: a core region, where the flow is irrotational and the fluid behaves like an inviscid fluid, and two boundary layers, where the flow is rotational and viscous effects are important. One boundary layer is located close the free surface and the other close to the bottom. A fair description of the flow in the core region can be obtained by assuming that the ratio $H = H^*/h^*$ between the height of the wave and the local water depth is a small quantity of the same order of magnitude as μ^2, where $\mu = h^*/L^*$ is the ratio between the water depth and a measure L^* of the length of the wave (Boussinesq approximation). Neglecting the damping of the wave, which takes place on a spatial scale much longer than L^*, and neglecting terms of order H^2, or equivalently of order μ^4, the free surface elevation η^* with respect to the still water level and the fluid velocity induced by the propagation of the wave can be evaluated by means of

$$\eta^*(X_1^*, t^*) = H^* \mathrm{sech}^2\left(\sqrt{\frac{3H}{4}}\zeta\right), \quad V_1^*(X_1^*, t^*) = H\sqrt{g^*h^*}\,\mathrm{sech}^2\left(\sqrt{\frac{3H}{4}}\zeta\right), \tag{2.1}$$

$$V_2^*(X_1^*, X_2^*, t^*) = -H^{3/2}\sqrt{3g^*h^*}\left(\frac{X_2^*}{h^*}\right)\mathrm{sech}^2\left(\sqrt{\frac{3H}{4}}\zeta\right)\tanh\left(\sqrt{\frac{3H}{4}}\zeta\right) \tag{2.2}$$

where $\zeta = (X_1^* - \sqrt{g^*h^*}t^*)/h^*$ and V_1^*, V_2^* are the horizontal and vertical velocity components, respectively (Grimshaw 1971).

At the leading order of approximation, the surface boundary layer can be neglected since it is much weaker than that located close to the bottom. To determine the flow close to the bottom, let us estimate the order of magnitude of the thickness δ^* of the bottom boundary layer, where viscous effects should balance the local inertial effects. The time development of V_1^* suggests that $\partial/\partial t^* \sim \sqrt{g^*h^*}/h^*$ while $\nu^*\partial^2/\partial x_2^{*2} \sim \nu^*/\delta^{*2}$, where ν^* is the kinematic viscosity of the sea water (hereinafter the scaling introduced by Grimshaw (1971) is used since it avoids the appearance of the parameter μ

into the problem). It follows that $\delta^* \sim \sqrt{\nu^* h^*/\sqrt{g^* h^*}}$ which, for actual waves, is much smaller than h^*. Therefore, introducing the boundary layer approximation, the continuity equation suggests that the vertical velocity component is negligible, the momentum equation in the vertical direction forces the pressure to be independent of the vertical coordinate and the horizontal velocity component v^*_{b1} in the boundary layer, which depends only parametrically on the coordinate X^*_1, can be obtained by solving

$$\frac{\partial v^*_{b1}}{\partial t^*} = \left.\frac{\partial V^*_1}{\partial t^*}\right|_{X_2=0} + \nu^* \frac{\partial^2 v^*_{b1}}{\partial X^{*2}_2} \tag{2.3}$$

where the streamwise pressure gradient term is replaced by $\partial V^*_1/\partial t^*|_{X^*_2=0}$. Of course, the flow field described by (2.3) should match the irrotational flow outside the boundary layer and satisfy the no-slip condition at the bottom. The solution of (2.3) can be found following the procedure described by Mei (1989, p. 564–569) and reads

$$v^*_{b1}(X^*_1, X^*_2, t^*) = V^*_1(X^*_1, t^*) \tag{2.4}$$

$$-H\sqrt{g^* h^*}\frac{2}{\sqrt{\pi}}\int_0^\infty \operatorname{sech}^2\left[\sqrt{\frac{3H}{4}}\left(\frac{X^{*2}_2}{2\delta^{*2}\xi^2} + \frac{X^*_1 - \sqrt{g^* h^*}t^*}{h^*}\right)\right] \mathrm{e}^{-\xi^2}\,\mathrm{d}\xi \tag{2.5}$$

where δ^* is defined by

$$\delta^* = \sqrt{\frac{2\nu^* h^*}{\sqrt{g^* h^*}}}. \tag{2.6}$$

3. The stability analysis

As already pointed out in the introduction, the analysis is aimed at analysing the stability of the basic flow in the bottom boundary layer. Indeed, the experimental visualizations of Sumer *et al.* (2010) suggest that, when the wave height is sufficiently large, the laminar regime in the boundary layer is unstable and two-dimensional perturbations appear. Hence, since we are focusing our attention close to the bottom, let us introduce the dimensionless variables

$$(x_1, x_2, x_3) = \frac{(X^*_1, X^*_2, X^*_3)}{\delta^*}, \quad t = \frac{t^*\sqrt{g^* h^*}}{h^*}. \tag{3.1}$$

Moreover, let us denote with (v_1, v_2, v_3) and p the dimensionless velocity components and the pressure field, respectively, defined by

$$(v_1, v_2, v_3) = \frac{(v^*_1, v^*_2, v^*_3)}{H\sqrt{g^* h^*}}, \quad p = \frac{p^*}{\rho^* H g^* \delta^*} \tag{3.2}$$

where ρ^* is the density of the sea water. Let us consider a two-dimensional perturbation of the flow field described by (2.4), such that

$$(v_1, v_2, p) = (v_{b1}, 0, p_b) + \epsilon(v_{p1}, v_{p2}, p_p) \tag{3.3}$$

where the dimensionless velocity $v_{b1} = v^*_{b1}/(H\sqrt{g^* h^*})$ can be easily obtained from (2.4). A linear analysis of the time development of the perturbation can be performed, if the amplitude ϵ of the perturbation is assumed to be much smaller than one. Assuming that $\epsilon \ll 1$ and neglecting term of order ϵ^2, continuity and momentum

equations read

$$\frac{\partial v_{p1}}{\partial x_1} + \frac{\partial v_{p2}}{\partial x_2} = 0 \tag{3.4}$$

$$\frac{\partial v_{p1}}{\partial t} + \frac{H}{\delta}\left[v_{b1}\frac{\partial v_{p1}}{\partial x_1} + v_{p2}\frac{\partial v_{b1}}{\partial x_2}\right] = -\frac{\partial p_p}{\partial x_1} + \frac{1}{2}\left[\frac{\partial^2 v_{p1}}{\partial x_1^2} + \frac{\partial^2 v_{p1}}{\partial x_2^2}\right] \tag{3.5}$$

$$\frac{\partial v_{p2}}{\partial t} + \frac{H}{\delta}\left[v_{b1}\frac{\partial v_{p2}}{\partial x_1}\right] = -\frac{\partial p_p}{\partial x_2} + \frac{1}{2}\left[\frac{\partial^2 v_{p2}}{\partial x_1^2} + \frac{\partial^2 v_{p2}}{\partial x_2^2}\right] \tag{3.6}$$

where the dimensionless parameter δ is defined by

$$\delta = \frac{\delta^*}{h^*}. \tag{3.7}$$

The continuity equation can be satisfied by introducing a stream function ψ such that

$$(v_{p1}, v_{p2}) = \left(\frac{\partial \psi}{\partial x_2}, -\frac{\partial \psi}{\partial x_1}\right). \tag{3.8}$$

By eliminating the pressure field from (3.5) and (3.6), the linearized vorticity equation is obtained

$$\frac{\partial^3 \psi}{\partial t \partial x_1^2} + \frac{\partial^3 \psi}{\partial t \partial x_2^2} + \frac{H}{\delta}\left[v_{b1}\left(\frac{\partial^3 \psi}{\partial x_1^3} + \frac{\partial^3 \psi}{\partial x_2^2 \partial x_1}\right) - \frac{\partial^2 v_{b1}}{\partial x_2^2}\frac{\partial \psi}{\partial x_1}\right] = \frac{1}{2}\left(\frac{\partial^4 \psi}{\partial x_1^4} + 2\frac{\partial^4 \psi}{\partial x_1^2 \partial x_2^2} + \frac{\partial^4 \psi}{\partial x_2^4}\right). \tag{3.9}$$

The linearity of (3.9) allows a normal mode analysis to be made and a generic spatial component along the x_1-axis to be considered. Since the height H^* of a solitary wave is usually much larger than the thickness δ^* of the viscous boundary layer, the value of the ratio H/δ turns out to be much larger than one. Simple algebra shows that the ratio H/δ is equal to the ratio between the characteristic temporal scale of the wave motion $h^*/\sqrt{g^* h^*}$ (see (3.1)) and the convective temporal scale characteristic of the time development of the perturbation $\delta^*/(H\sqrt{g^* h^*})$ (the latter is assumed to be equal to the ratio between the thickness of the bottom boundary layer and the scale of the fluid velocity; see (3.2)). Hence, the amplitude of the perturbation can be supposed to grow on a time scale much faster than that which characterizes the time development of the basic flow and a 'momentary' criterion for instability of the kind introduced by Shen (1961) and discussed by Blondeaux & Seminara (1979) can be used. Therefore, the function ψ can be written in the form

$$\psi(x_1, x_2, t) = \mathrm{Re}\left\{f(x_2, t)\exp\left[\mathrm{i}\alpha\left(x_1 - \frac{H}{\delta}\int c(\tau)\,\mathrm{d}\tau\right)\right]\right\} + \text{h.o.t.} \tag{3.10}$$

where α indicates the streamwise wavenumber of the generic Fourier component of the perturbation, the real part (c_r) of c is its wave speed and the imaginary part (c_i) controls its growth/decay. Moreover, h.o.t. indicates higher order terms. Substitution of (3.10) into (3.9) leads to the following homogeneous differential equation

$$[v_{b1}(x_2, t) - c(t)]N^2 f(x_2, t) - \frac{\partial^2 v_{b1}(x_2, t)}{\partial x_2^2} f(x_2, t) = \frac{1}{2\mathrm{i}\alpha(H/\delta)} N^4 f(x_2, t) \tag{3.11}$$

where the operator N^2 is defined by $N^2 = (\partial^2/\partial x_2^2) - \alpha^2$.

Moreover, the boundary conditions force the vanishing of the velocity at the wall and far from the bottom. Let us point out that the viscous term, which is of order $1/(H/\delta)$, is retained in (3.11), since it turns out to be significant, at the leading order of approximation, within a viscous layer close to the wall and within possible critical layers. A more formal approach would require, first, the solution of the inviscid version of (3.11). Then, the inviscid solution should be matched with the solution in the viscous and critical layers. Such a procedure would involve a lot of tedious and heavy algebra and the direct solution of the (3.11) has thus been preferred. In a similar context, Blondeaux & Vittori (1994) showed that the solution of (3.11) coincides, to the required order of approximation, with the solution obtained on the basis of the rigorous matched asymptotic approach previously outlined. We also note that the time variable t^* and the spatial variable X_1^* appear into the problem only in the combination $\zeta = X_1 - t$, which can be considered as a parameter of the problem and (3.11) can be solved for different values of ζ which correspond to different locations and/or to different phases within the wave cycle. In the following we consider the location characterized by $X_1 = 0$, such that a vanishing value of ζ corresponds to the passage of the wave crest at the considered location.

In order to find a non-vanishing solution of the homogeneous differential problem posed by (3.11) and its boundary conditions, it is necessary to force an eigenrelation which provides the value of c as function of α and the other parameters of the problem. To find the largest eigenvalue c and the corresponding eigenfunction f, a numerical approach is used. Equation (3.11) and its boundary conditions are discretized by a fourth-order compact finite difference approach along the x_2-direction. The outer boundary is set at $x_2 = 30$, where the standard asymptotic conditions of inviscid outer behaviour are forced. The least stable eigenvalue is obtained by inverse iteration. To check the numerical solution, (3.11) is solved also by a spectral collocation procedure. Any desirable precision can be obtained choosing a sufficient number of grid nodes in the finite difference approach and Chebyshev collocation points in the spectral one.

4. Discussion of the results

The eigenvalue problem formulated in the previous section depends on the ratio H/δ, the dimensionless wave height H, which appears in the basic flow described by (2.4), and the parameter ζ. In the following, the eigenrelation and the eigensolution are determined for fixed values of δ and H and by varying the phase within the wave cycle, since the value of the coordinate X_1^* is considered fixed and equal to zero.

Figure 1(*a*) shows the temporal dependence of the growth rate c_i of the harmonic component characterized by $\alpha = 0.20$, for $H = 0.12$ and $\delta = 5.0 \times 10^{-4}$, which are the values of the parameters of the experiment of Sumer *et al.* (2010) characterized by a maximum value of the free stream velocity $U_{0m}^* = 50.9$ cm s^{-1} and $T^* = 4\pi h^*/\sqrt{3g^*H^*} = 9.3$ s ($Re = 3.8 \times 10^5$). The value $\alpha = 0.20$ has been chosen because it is the critical wavenumber, i.e. it corresponds to the Fourier component which is first destabilized. During the accelerating phase, i.e. for negative values of ζ, the value of c_i turns out to be smaller than zero and the perturbation component tends to decay. The value of c_i remains negative during the early decelerating phases showing that the mode is stable also after the passage of the wave crest. However, as soon as ζ becomes larger than about $\zeta = 1.0$, the value of c_i becomes positive and the mode characterized by a wavenumber equal to 0.20 tends to grow. Figure 1(*b*) shows the value of c_r, which is related to the migration speed of the perturbation component.

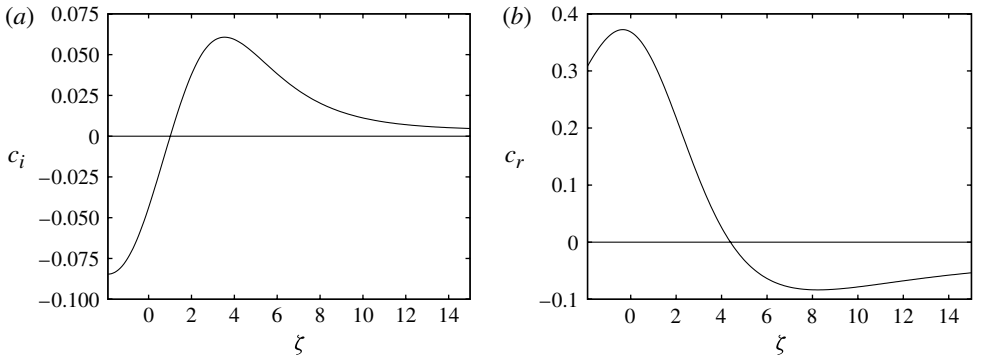

FIGURE 1. Growth rate c_i (a) and phase velocity c_r (b) plotted versus ζ for $\alpha = 0.20$, $H = 0.12$ and $\delta = 5.0 \times 10^{-4}$.

Up to about $\zeta = 4.4$, the value c_r is positive, thus indicating that the perturbation component migrates in the direction of wave propagation. Only for values of ζ larger than 4.4 does c_r become negative showing that the perturbation component reverses its velocity at the late decelerating phase because of flow reversal within the boundary layer.

Similar results are found for different values of α and an exhaustive picture of the phenomenon is provided by figure 2, which shows the value of c_i as a function of ζ and α for the same values of H and δ as those considered in figure 1. A region in the plane (ζ, α) is present, which is characterized by positive values of c_i. If the fastest growing mode is assumed to prevail on the other modes, the stability analysis predicts the appearance of a periodic pattern characterized by a wavelength ℓ^* such that $2\pi\delta^*/\ell^*$ equals the value $\hat{\alpha}$ of α which gives rise to the maximum growth rate for a given value of ζ. Moreover, a periodic pattern is predicted to appear for $\zeta > \zeta_c$, i.e. as soon as c_i becomes positive. Owing to the slow temporal variation of the basic flow, the dimensionless wavelength ℓ^*/δ^* of the most unstable harmonic component depends on the phase within the wave cycle. Hence, the periodic pattern, the appearance of which is predicted by the analysis, would be characterized by a wavelength which depends on time. However, the perturbation wavelength cannot change in a continuous way but only through the appearance of defects (e.g. dislocations) and their growth. The dynamics of these defects cannot be investigated by means of a linear analysis and, in the following, it is assumed that the wavelength of the periodic pattern which is expected to appear is coincident with that predicted at $\zeta = \zeta_c$. This qualitative conclusion is supported by an analysis of the experiments made by Sumer *et al.* (2010), the movies of which are available at http://dx.doi.org/10.1017/S0022112009992837 in the supplementary material of that paper. Indeed, the movies do not show any significant change of the distance between adjacent vortex tubes during their time development. The results of figure 2 show that ζ_c is equal to $\sim$1.0 and $\hat{\alpha}$ evaluated at $\zeta = \zeta_c$, which is denoted by α_c, is equal to $\sim$0.20. To ascertain the reliability of the analysis, the theoretical findings have been compared with the experimental measurements of Sumer *et al.* (2010). Indeed, the flow visualizations of Sumer *et al.* (2010) allow an estimate of the wavelength of the most unstable perturbation component to be obtained, if the growth of the latter is assumed to give rise to the vortex tubes observed in the experiments. For $U^*_{0m} = 50.9$ cm s^{-1} and $T^* = 9.3$ s, the average distance between the axes of adjacent vortex tubes visualized by Sumer *et al.* (2010) is $\sim$2.3 cm, a value which corresponds

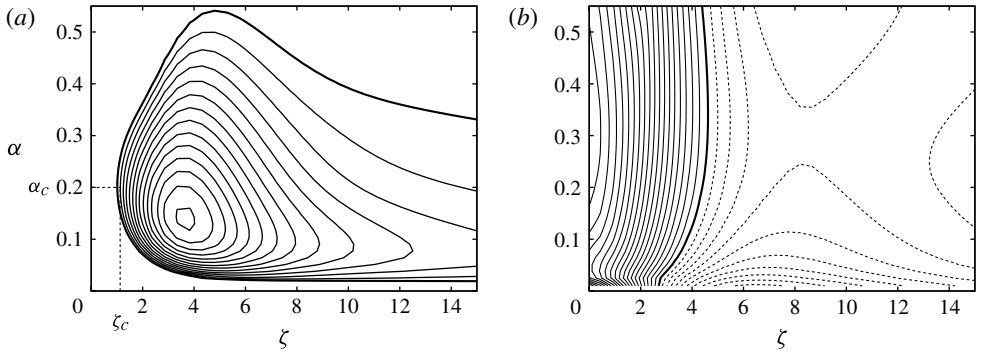

FIGURE 2. (*a*) Growth rate c_i (continuous line, $c_i > 0$; continuous thick line, $c_i = 0$; $\Delta c_i = 0.005$) and (*b*) phase velocity c_r (continuous lines, $c_r > 0$; broken lines $c_r < 0$, continuous thick line $c_r = 0$; $\Delta c_r = 0.02$) plotted versus ζ and α for $H = 0.12$ and $\delta = 5.0 \times 10^{-4}$.

Movie	U_{0m}^* (cm s^{-1})	T^* (s)
1	50.9	9.3
2	43.9	9.2
3	93.9	7.8
4	36.2	9

TABLE 1. Values of U_0^* and T^* characterizing the movies of the experiments made by Sumer *et al.* (2010).

to α_c equal to $\sim$0.24. Moreover, a periodic pattern can be identified 1.53 s after the free stream velocity attains its maximum, i.e. at $\zeta = 3.18$. A fair agreement between the theoretical predictions and the experimental measurements is found as far as the wavelength of the most unstable mode is considered. On the other hand, the value of ζ at which the periodic patterns are observed in the experiments is significantly larger than that predicted by the stability analysis. This can be explained considering that the perturbation, which starts to grow, takes some time to attain an amplitude large enough to be detected visually. The theoretical predictions are compared with all of the flow visualizations which are available at http://dx.doi.org/10.1017/S0022112009992837 and with a further movie which has been made available by the experimentalists. The values of the experimental parameters are given in table 1.

The agreement between the predicted and observed wavenumbers is satisfactory, even though the predictions (α_c equal to 0.20, 0.20, 0.21 and 0.205 for movies 1–4, respectively) slightly underestimate observed values which fall in the ranges (0.21, 0.30), (0.23, 0.30), (0.23, 0.27) and (0.19, 0.26), respectively. On the other hand, as already pointed out, the predicted values of ζ_c, which are equal to 1.01, 1.16, 0.53 and 1.39 are significantly smaller than the observed values which are 3.18, 4.77, 2.23 and 4.81.

The direct numerical simulations of Vittori & Blondeaux (2008, 2011) show that turbulence appearance is observed when the parameter H is larger than a critical value H_c, which increases as δ is increased. This behaviour of $H_c(\delta)$ was observed also in the experiments of Sumer *et al.* (2010), who defined the Reynolds number

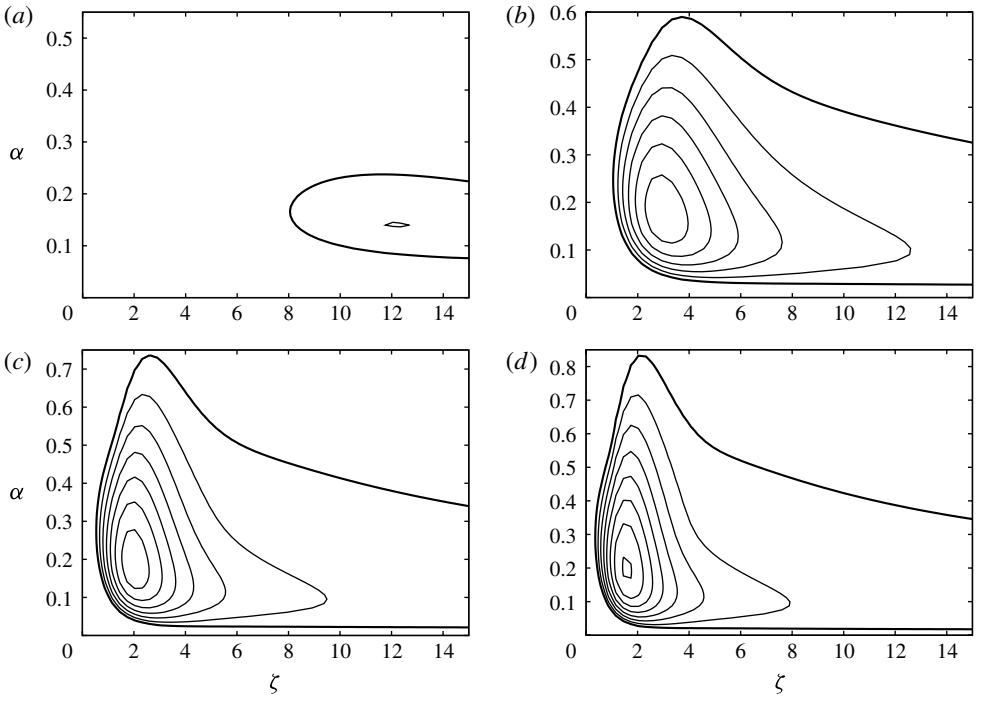

FIGURE 3. Growth rate c_i (continuous line, $c_i > 0$; continuous thick line $c_i = 0$; $\Delta c_i = 0.01$) plotted versus ζ and: α for $\delta = 1.2 \times 10^{-3}$ and: (*a*) $H = 0.025$; (*b*) $H = 0.2$; (*c*) $H = 0.4$; (*d*) $H = 0.6$.

as $Re = 4H^{3/2}/(\sqrt{3}\delta^2)$ and proposed a critical value equal to 2×10^5, to discriminate between the stable laminar regime and a transitional flow, i.e. a flow characterized by the presence of 'regular' two-dimensional vortex tubes. Even though the qualitative behaviour of the results of the present stability analysis agrees with that found by Vittori & Blondeaux (2008) and Sumer *et al.* (2010), significant quantitative differences are found. Indeed, the present stability analysis indicates instability of the laminar regime for values of H smaller than those predicted numerically and/or observed experimentally. For example, for $\delta = 1.2 \times 10^{-3}$, the theoretical results show that H_c falls around 0.025 (see figure 3), a value which is much smaller than that proposed by Sumer *et al.* (2010) and observed by Vittori & Blondeaux (2008). This finding can be understood looking at figure 4, which shows results obtained by means of direct numerical simulations made with the same code used by Vittori & Blondeaux (2008). In particular, figure 4 shows the dimensionless kinetic energy per unit area K of the flow perturbations plotted versus the phase ζ within the wave cycle for $\delta = 1.2 \times 10^{-3}$ and different values of H. For $H = 0.025$ the value of K is negligible during the whole wave cycle as predicted by the present linear stability analysis (see figure 3*a*). If H is slightly increased, K grows during the late decelerating phase as predicted by the present linear stability analysis. However, up to $H = 0.4$, the growth of K is weak and does not lead to the appearance of detectable perturbations of the velocity field which is practically coincident with that predicted by (2.4). Only when H is equal to 0.5 or larger, the strength attained by the perturbations is significant and the flow deviates from the laminar flow. Of course, the process is continuous and

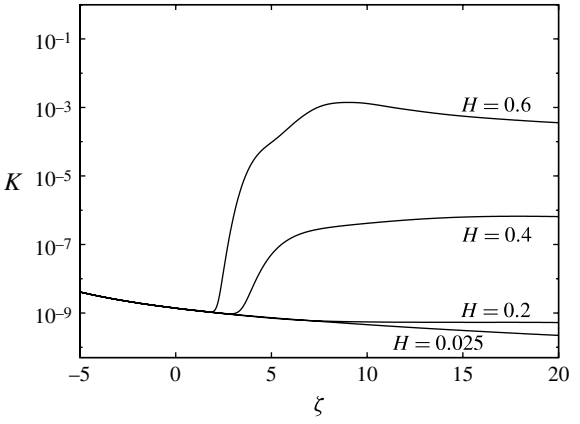

FIGURE 4. Dimensionless kinetic energy K of flow perturbations plotted versus ζ for $\delta = 1.2 \times 10^{-3}$ and different values of H.

there is some arbitrariness in defining the value of H which gives rise to significant perturbations. Indeed both Vittori & Blondeaux (2008, 2011) introduced an arbitrary threshold value of K to discriminate between the laminar and the turbulent regimes. The results plotted in figure 4 explain also the differences between the values of ζ_c predicted by the present stability analysis and those at which Sumer *et al.* (2010) observed vortex tubes. Indeed, figure 4 shows that there is a significant time delay between the beginning of the growth of the perturbations and the phase at which they attain a significant level. When comparing the present theoretical results with the numerical finding of Vittori & Blondeaux (2008) and the experimental measurements of Sumer *et al.* (2010), the reader should consider that for small values of H the stability analysis is not expected to provide accurate quantitative results because the ratio H/δ is not large enough in order to reliably apply a 'momentary' criterion for instability. An important issue which needs to be ascertained is whether the instability predicted by the present analysis is convective or absolute. Since the characteristic horizontal length scale of a solitary wave is much larger than the thickness of the viscous boundary layer, the basic flow can be assumed to be slowly varying in the streamwise direction. Hence, the approach proposed by Huerre & Monkewitz (1990) can be used to investigate the absolute/convective character of the predicted instability. A perturbation characterized by a complex wavenumber which leads to a vanishing group velocity has been searched by means of an iterative procedure by varying the phase within the wave cycle and considering different values of the parameters of the problem. Huerre & Monkewitz (1990) suggest that the instability is absolute if the growth rate of such perturbation is positive. On the other hand, the instability is convective if the growth rate is negative. In the range of the parameters presently investigated no absolute instability is found and no global instability can exist. This finding differs from that of Bogucki & Redekopp (1999) who considered an internal solitary wave and showed that the separated region which appears in the boundary layer under the wave might be globally unstable.

5. Conclusions

The stability analysis described in § 3 and the results discussed in § 4 show that the laminar boundary layer at the bottom of a solitary wave, propagating over a constant

water depth, is unstable if the height of the wave exceeds a threshold value which depends on the thickness of the boundary layer. For example, figure 3 shows that, for $\delta = 1.2 \times 10^{-3}$, the threshold value of H is close to 0.025, since for smaller values of H the growth rate c_i turns out to be negative for any value of α and ζ. In the range of the parameters presently investigated, the instability takes place during the decelerating phase of the wave cycle. The wavelength of the fastest growing mode, at the critical conditions, is found to be similar to the distance between the adjacent vortex tubes observed experimentally by Sumer *et al.* (2010). A comparison of the theoretical results with the numerical findings of Vittori & Blondeaux (2008) and the experimental visualizations of Sumer *et al.* (2010) seems to indicate that the stability analysis underpredicts the threshold value of the wave height triggering the instability of the laminar regime. However, a careful analysis of the results shows that the discrepancy between the predictions of the linear stability analysis and the numerical/experimental results can be explained by considering the unsteady character of the basic flow which does not allow a significant growth of the perturbation to be attained during the early stages of the instability.

Acknowledgements

This study has been funded by the 'Ministero dell'Istruzione, dell'Universitá e della Ricerca' under the research project 2008YNPNT9-003 'Idrodinamica e morfodinamica nella regione dei frangenti'. The authors thank Professor Sumer and Dr Carstensen who made available a movie of the experiments and measurements of the characteristics of the vortex tubes.

REFERENCES

BLONDEAUX, P. 1987 Turbulent boundary layer at the bottom of gravity waves. *J. Hydraul. Res.* **25** (4), 447–464.

BLONDEAUX, P. & SEMINARA, G. 1979 Transizione incipiente al fondo di un'onda di gravitá. *Acc. Naz. Lincei* **67**, 408–411 (*italian*).

BLONDEAUX, P. & VITTORI, G. 1994 Wall imperfections as a triggering mechanism for Stokes-layer transition. *J. Fluid Mech.* **264**, 107–135.

BLONDEAUX, P. & VITTORI, G. 1999 Boundary layer and sediment dynamics under sea waves. *Adv. Coast Ocean Engng* **4**, 133–190.

BLONDEAUX, P. & VITTORI, G. 2012 RANS modelling of the turbulent boundary layer under a solitary wave. *Coast. Engng* **60**, 1–10.

BOGUCKI, D. J. & REDEKOPP, L. G 1999 A mechanism for sediment resuspension by internal solitary waves. *Geophys. Res. Lett.* **26** (9), 1317–1320.

CONRAD, P. W. & CRIMINALE, W. O. 1965 The stability of time-dependent laminar flows. *Z. Angew. Math. Phys.* **16**, 233–254.

COSTAMAGNA, P., VITTORI, G. & BLONDEAUX, P. 2003 Coherent structures in oscillatory boundary layers. *J. Fluid Mech.* **474**, 1–33.

FREDSOE, J. & DEIGAARD, R. 1992 *Mechanics of Coastal Sediment Transport*, *Advanced Series on Ocean Engineering*, vol. 3. World Scientific.

GRIMSHAW, R. 1971 The solitary wave in water of variable depth. Part 2. *J. Fluid Mech.* **46** (3), 611–622.

HUERRE, P. & MONKEWITZ, P. A. 1990 Local and global instabilities in spatially developing flows. *Annu. Rev. Fluid Mech.* **22**, 473–537.

LIU, P. L. F. & ORFILIA, A. 2004 Boundary layer hydrodynamics and bed load sediment transport in oscillating water tunnels. *J. Fluid Mech.* **520**, 83–92.

LIU, P. L. F., PARK, Y. S. & COWEN, E. A. 2007 Boundary layer flow and bed shear stress under a solitary wave. *J. Fluid Mech.* **574**, 449–463.

MAZZUOLI, M., VITTORI, G. & BLONDEAUX, P. 2011 Turbulent spots in oscillatory boundary layers. *J. Fluid Mech.* **685**, 365–376.

MEI, C. C. 1989 *The Applied Dynamics of Ocean Surface Waves*, *Advanced Series on Ocean Engineering*, vol. 1. World Scientific.

SHEN, S. F. 1961 Some considerations on the laminar stability of incompressible time-dependent basic flows. *J. Aerosp. Sci.* **28**, 397–404 and 417.

SUMER, B. M., JENSEN, P. M., SORENSEN, L. B., FREDSOE, J., LIU, P. L. F. & CARSTENSEN, S. 2010 Coherent structures in wave boundary layers. Part 2. Solitary motion. *J. Fluid Mech.* **646**, 207–231.

TANAKA, H., SUMER, B. M. & LODAHL, C. 1998 Theoretical and experimental investigation on laminar boundary layers under cnoidal wave motion. *Coast. Engng J.* **40** (1), 81–98.

VERZICCO, R. & VITTORI, G. 1996 Direct simulation of transition in Stokes layers. *Phys. Fluids* **8** (6), 1341–1343.

VITTORI, G. 2003 Sediment suspension due to waves. *J. Geophys. Res. Oceans* **108** (C6), 3173 4-1/4-17.

VITTORI, G. & BLONDEAUX, P. 2008 Turbulent boundary layer under a solitary wave. *J. Fluid Mech.* **615**, 433–443.

VITTORI, G. & BLONDEAUX, P. 2011 Characterstics of the boundary layer at the bottom of a solitary wave. *Coast. Engng* **58** (2), 206–213.

VITTORI, G. & VERZICCO, R. 1998 Direct simulation of transition in an oscillatory boundary layer. *J. Fluid Mech.* **371**, 207–232.

TALMON, A. M., STRUIKSMA, N. & VAN MIERLO, M. C. L. M. 1995 Laboratory measurements of the direction of sediment transport on transverse alluvial-bed slopes. *J. Hydraul. Res.* **33**, 495–517.